JACS
JOURNAL OF THE AMERICAN CHEMICAL SOCIETY

Article

pubs.acs.org/JACS

Monomolecular Siloxane Film as a Model of Single Site Catalysts

Michael W. Martynowycz,[†,§] Bo Hu,[‡,⊥] Ivan Kuzmenko,[*,§] Wei Bu,[∥] Adam Hock,[*,‡,§] and David Gidalevitz[*,†]

[†]Center for the Molecular Study of Condensed Soft Matter and Department of Physics, [‡]Department of Chemistry, Illinois Institute of Technology, Chicago, Illinois 60616, United States

[§]Argonne National Laboratory, Lemont, Illinois 60439, United States

[∥]Center for Advanced Radiation Sources, University of Chicago, Chicago, Illinois 60637, United States

Supporting Information

ABSTRACT: Achieving structurally well-defined catalytic species requires a fundamental understanding of surface chemistry. Detailed structural characterization of the catalyst binding sites *in situ*, such as single site catalysts on silica supports, is technically challenging or even unattainable. Octadecyltrioxysilane (OTOS) monolayers formed from octadecyltrimethoxysilane (OTMS) at the air−liquid interface after hydrolysis and condensation at low pH were chosen as a model system of surface binding sites in silica-supported Zn^{2+} catalysts. We characterize the system by grazing incidence X-ray diffraction, X-ray reflectivity (XR), and X-ray fluorescence spectroscopy (XFS). Previous X-ray and infrared surface studies of OTMS/OTOS films at the air−liquid interface proposed the formation of polymer OTOS structures. According to our analysis, polymer formation is inconsistent with the X-ray observations and structural properties of siloxanes; it is energetically unfavorable and thus highly unlikely. We suggest an alternative mechanism of hydrolysis/condensation in OTMS leading to the formation of structurally allowed cyclic trimers with the six-membered siloxane rings, which explain well both the X-ray and infrared results. XR and XFS consistently demonstrate that tetrahedral $[Zn(NH_3)_4]^{2+}$ ions bind to hydroxyl groups of the film at a stoichiometric ratio of OTOS:Zn ∼ 2:1. The high binding affinity of zinc ions to OTOS trimers suggests that the six-membered siloxane rings are binding locations for single site Zn/SiO_2 catalysts. Our results show that OTOS monolayers may serve as a platform for studying silica surface chemistry or hydroxyl-mediated reactions.

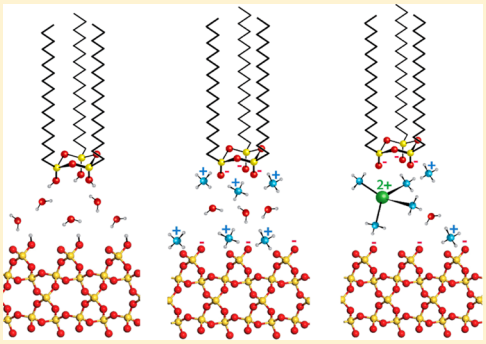

1. INTRODUCTON

Recent work has shown that ions of zinc, cobalt, and iron bound to amorphous silica are stable and highly selective catalytic materials for the generation of propene through propane dehydrogenation.[1−3] *In situ* studies of metal ions interacting with the surface of amorphous silica by extended X-ray absorption fine structure or X-ray absorption near edge structure are complicated by simultaneous X-ray sampling of the bulk, ion-rich solutions. Conventional surface spectroscopic methods are also insufficient for near-atomic structural characterization of binding during the adsorption process. Thus, structural determination of the metal−silica interface appears hard or even unattainable by conventional methods.

Langmuir monolayers are unimolecular films that self-assemble at the air−liquid interface. Due to their flat geometry, these films are advantageous for structural studies at interfaces. The structure of Langmuir monolayers can be established at near-atomic resolution using a liquid surface spectrometer at a synchrotron X-ray source.[4] Here, we present a model system for studying the adsorption of zinc ions on silica surfaces. Octadecyltrimethoxysilane (OTMS) and its close analogs at the air−liquid interface undergo hydrolysis and condensation at low pH, forming a monolayer of octadecyltrioxysilane (OTOS, Figure 1A).[5−16] Since OTOS has free hydroxyl groups, we chose OTOS to model the silica surface in metal-ion silica-supported catalysts.[17] We discuss our data and compare it with the results of previous studies on condensed OTMS films. We demonstrate that previous structural models of OTOS/OTMS films are impossible due to limitations of molecular geometry and crystallographic constraints. We propose an alternative molecular model of the OTOS film with well-defined geometry and symmetry that explains both our results and previously published data. According to this model, OTOS forms trimers in which one oxygen terminates in a free hydroxyl whereas the two other oxygens form silicon−oxygen−silicon bonds with neighbors (Figure 1).

Using specular X-ray reflectivity (XR), grazing incidence X-ray diffraction (GIXD), and X-ray fluorescence spectroscopy (XFS), we demonstrate that zinc ions bind to the head groups of the OTOS monolayer. Furthermore, surface XFS indicates that zinc ions bind to the interface at ∼2:1 hydroxyl to zinc ratio. It was suggested that the surface structures on solid supports responsible for zinc adsorption were hydroxyl defect

Received: June 3, 2016
Published: September 6, 2016

ACS Publications © 2016 American Chemical Society

DOI: 10.1021/jacs.6b05711
J. Am. Chem. Soc. 2016, 138, 12432−12439

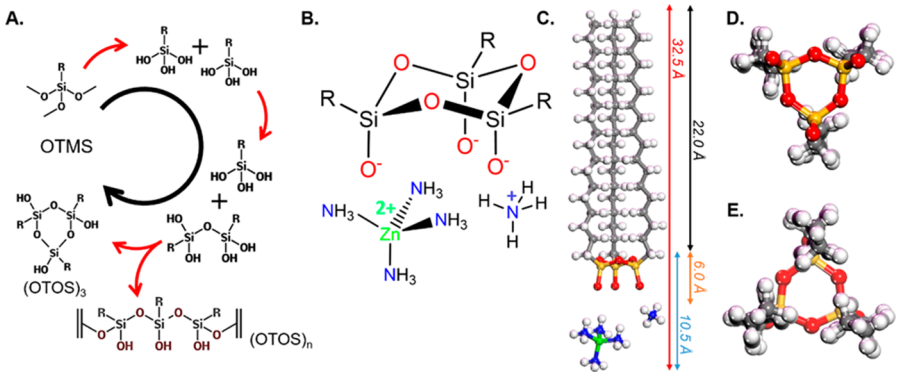

Figure 1. (A) OTMS hydrolysis followed by condensation may lead either to formation of linear polymers or to cyclic trimers of OTOS. (B) Schematic representation of the OTOS trimer and its interactions with zinc ions via the terminal oxygens. (C) Molecular model of a single OTOS trimer at the air−liquid interface (side view), showing lengths of different molecular regions, in agreement with the X-ray reflectivity results. OTOS trimer (D) viewed from the bottom and (E) viewed from the top.

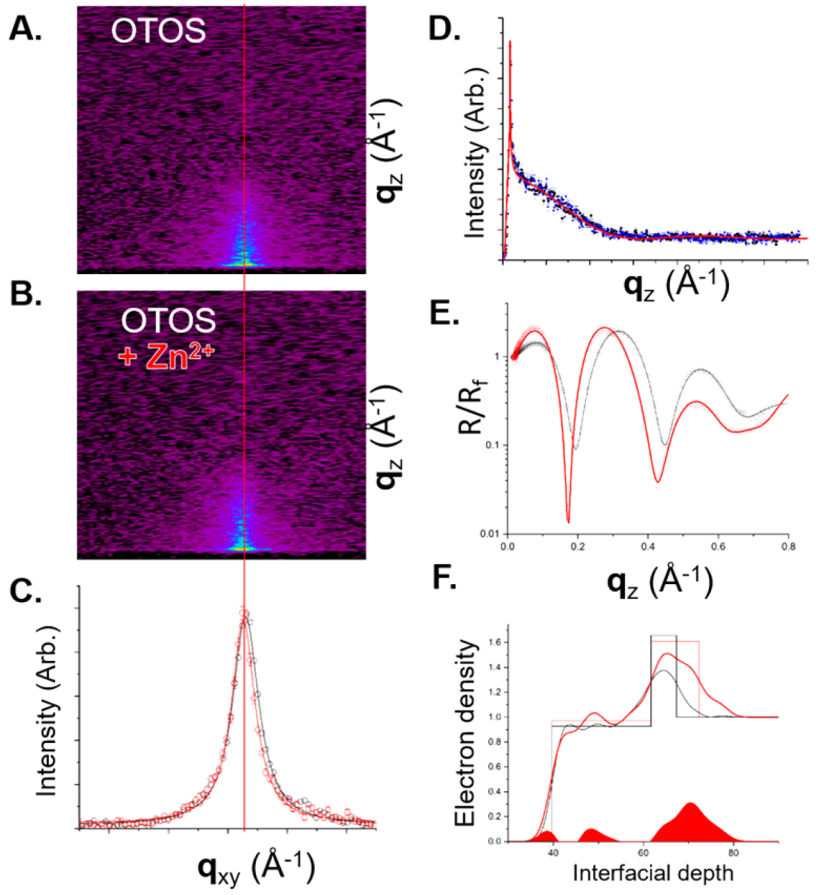

Figure 2. Grazing incidence X-ray diffraction intensity distribution maps of the main region of interest in q_{xy} from (A) an OTOS film at the air−liquid interface and (B) an OTOS film after the addition of Zn^{2+} to the subphase. (C) Corresponding diffraction patterns integrated over q_z. Vertical red lines indicate the q_{xy} position of the intensity maxima; they overlap within experimental error. (D) Overlapping Bragg rod profiles obtained by integration over q_{xy} of patterns A (black dots) and B (blue dots) with the model fit (red line), which well describes both data sets. (E) Fresnel-normalized specular X-ray reflectivity from the OTOS film (black) and after the addition of Zn^{2+} (red). (F) Electron density profiles of the OTOS film before (black curve) and after (red curve) the addition of Zn^{2+} ions, generated using stochastic tunneling for a model independent fit with square boxes giving the general regions of electron density of the film. The Fourier "wiggles" in the chain region appear due to the limited range of reflectivity measurements and are related to a finite number of Fourier orders.

sites in the six-membered silicon oxide rings. According to our results, Zn^{2+} binds to the OH groups of the film, thus providing support that Zn^{2+} is present in the surface defects of amorphous silica catalysts.[3]

2. RESULTS AND DISCUSSION

2.1. Structure of OTMS/OTOS Films Based on GIXD and XR. As reported previously, at low pH, an OTMS monolayer on the aqueous subphase undergoes hydrolysis and condensation, resulting in an ordered OTOS monolayer film

DOI: 10.1021/jacs.6b05711
J. Am. Chem. Soc. 2016, 138, 12432−12439

Table 1. Grazing Incidence X-ray Diffraction Analysis

	q_{xy} maxima (Å^{-1} ± 0.01)	d-spacing (Å ± 0.005)	full width at half-maximum (Å^{-1} ± 0.01)	unit cell area (Å^2 ± 0.05)	coherence length[a] (Å ± 10)
OTOS	1.530	4.11	0.053	19.47	133
OTOS + $[Zn(NH_3)_4]^{2+}$	1.526	4.12	0.047	19.57	152

[a]Coherence length of the crystalline domains is given by the Sherrer formula (see Experimental Section).

with hexagonal symmetry.[9,15,16] The GIXD spectrum of the OTOS monolayer film at a surface pressure of 45 mN m^{-1} is given by a single diffraction peak at q_{xy} = 1.53 Å^{-1} (Figure 2A), corresponding to a hexagonal unit cell with $a = b$ = 4.8 Å and γ = 120° (Table 1). A hexagonal motif is one of the typical packing modes of hydrocarbon chains in Langmuir films.[18,19] Both the position and width of the triple degenerate peak {(10) + (01) + (1−1)} are compatible with the previously reported GIXD results for condensed OTMS films. Our interpretation of these results, however, is significantly different.

It has been repeatedly suggested by several groups that siloxane groups of the OTMS monolayer form either 1D or 2D polymers upon hydrolysis/condensation.[7−16,20] Below, we provide arguments that neither linear nor 2D polymer networks are likely to form ordered monolayer structures under these conditions due to structural and symmetry limitations, as given by the known molecular geometry and GIXD/XR analysis. According to our query of the Cambridge Structural Database (see the Supporting Information), the typical Si···Si distance of the Si−O−Si unit in organosilicates is 3.10 ± 0.05 Å, with a typical Si−O distance of 1.62 ± 0.02 Å and Si−O−Si angle of 147 ± 8° (Figure 3). Thus, the maximum Si···Si repeat distance in the $(Si−O−Si)_n$ polymer chain cannot exceed 3.2 Å (the double of Si−O distance). Such a polymer chain is incommensurate with the 4.8 Å repeat distance in the nearest-neighbor (NN) direction of the crystalline structure, nor is it commensurate with a next-nearest-neighbor (NNN) distance of 4.2 Å (Figure 3). The difference between total $(Si−O−Si)_n$ polymer chain length and the corresponding crystallographic repeat distance ($n \times 1.7$ Å for NN or $n \times 1.1$ Å for NNN) grows proportional to the number of the repeat units. Even the third in a row of silicate headgroup belonging to either NN or NNN may only reach to form another (Si−O−Si)−O−Si bond if part of the attached hydrocarbon chain is partially pulled into the subphase to bridge the gap (dashed yellow line in Figure 3). Such a scenario is both energetically unfavorable and inconsistent with the X-ray scattering results. It is energetically unfavorable as it requires the hydrophobic chain to be partially removed from the hydrophobic environment of the neighboring chains and inserted into the aqueous medium. It is inconsistent with the X-ray data as both the width of the Bragg rods in GIXD and the electron density profile obtained from the XR data support the model of a monolayer of uniform thickness in which the hydrocarbon tails are almost fully stretched and aligned normal to the surface. The only possibility for the $(Si−O−Si)_n$ linear polymerization in the film, given the structural limitations, is a polymer chain that runs in the NN direction in a zigzag fashion, stitching two neighboring rows of hydrocarbon chains, as shown in Figure 4A. This motif, suggested previously by Sjöblom et al. (see Figure 15),[20] appears to be the only feasible linear polymerization product that satisfies both the Si−O−Si geometry and intermolecular distances between hexagonally packed hydrocarbon chains. Given the constraints, other modes of 1D or 2D polymerization within the film are geometrically impossible. Even though viscosity measurements performed on the condensed OTMS films seemed to support the formation of 2D polymers,[14,22] the interpretation of these results is not straightforward, and a model of the 2D polymer of satisfactory molecular geometry was never proposed. Moreover, studies of nonpolymerized Langmuir films of high (hexagonal) symmetry demonstrated rather high viscosity values.[23]

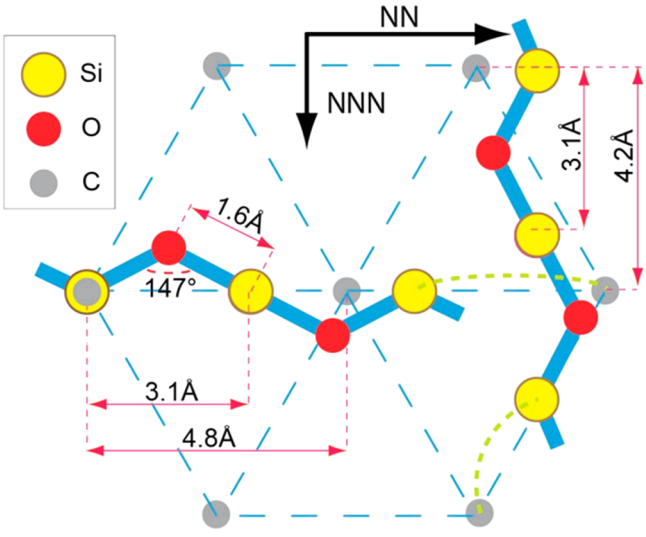

Figure 3. Top schematic view of hydrocarbon chains (gray circles) packed in a hexagonal lattice. The Si···Si repeat distances of 3.1 Å in the silica polymer chain are incompatible with the periodicity of the hydrocarbon chains in either nearest-neighbor (NN) or next-nearest-neighbor (NNN) directions with periods of 4.8 and 4.2 Å, respectively. The yellow dashed lines show impossibly long Si···C bond covalent distances arising between the third in a row of O and C atoms that must be satisfied; the average bond distances and angles in the Si−O−Si moiety were obtained from 3D structures of organosilanes from the Cambridge Structure Database (CSD).

The only structurally allowed 1D polymerization motif remains at odds with the GIXD results. The 2D crystal of OTOS built of such polymers, as shown in Figure 4C, does not possess 3-fold symmetry since the d-spacings along the covalently bound hydrocarbon chains ($d_1 = d_2$) and the corresponding van der Waals spacing between the neighboring polymers (d_3) are not symmetry related and thus should not be the same. In other words, a GIXD pattern corresponding to such a structure would result in two distinct Bragg peaks, corresponding to a centered rectangular unit cell, not a triple-degenerate Bragg peak.[19] We, therefore, propose that the only feasible molecular OTOS model, consistent with the GIXD and XR data, is a cyclic trimer, as shown in Figures 1C−E and 4B,D. The OTOS cyclic trimer, which is obtained from OTMS through hydrolysis and condensation (Figure S4), has satisfactory inter- and intramolecular contacts. There are analogs of the OTOS trimer that were characterized structurally

DOI: 10.1021/jacs.6b05711
J. Am. Chem. Soc. 2016, 138, 12432−12439

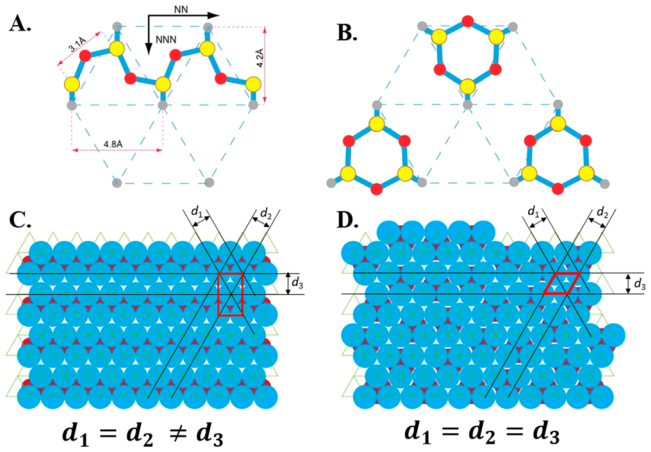

Figure 4. (A) Schematic top-view representation of the formerly proposed OTOS monolayer structure overlaid onto the hexagonal structure of the hydrocarbon chains. The 1D polymer structure conforms with the periodicity of the acyl chains in the nearest-neighbor (NN) direction by forming a zigzag. (B) Alternative OTOS structure, made of cyclic trimers, compatible with the hexagonal packing of hydrocarbon chains that also satisfies the typical Si···Si distances. (C) Hypothetical 2D packing of 1D OTOS polymers; underlying $(-Si-O-Si-)_n$ chains are marked in dark red. The orthorhombic symmetry of such a crystalline film ($d_1 = d_2 \neq d_3$) is incompatible with the observed diffraction data. (D) OTOS monolayer structure built of cyclic trimers of two opposite orientations that are likely to be distributed aperiodically within the film. The long-range order is maintained for the hydrocarbon chains only (solid blue circles). The overall symmetry of the film is hexagonal ($d_1 = d_2 = d_3$).

in bulk crystals; examples are given by the CSD database (see the Supporting Information). Our trimer model also agrees with the polarization-modulated infrared reflection absorption spectroscopy (PM-IRRAS) study by Blaudez et al.[11] According to their results, about one-third of Si−OH groups of OTOS remain upon condensation, whereas the rest convert into the −Si−O−Si− state. The polymer model of the OTOS monolayer structure suggested by Carino et al.[15] assumed 50% Si−O−Si bond formation and is inconsistent with the PM-IRRAS results. We remark that Ulman (Figure 3 in Ulman, 1990)[5] described the possibility of siloxane cyclic trimer formation in the bulk, but it was never considered as the main structural module of the condensed OTMS films. Assuming that the trimer is the main unit of the 2D monolayer structure, we also suggest that the film does not have long-range order for the whole trimer, but only for the hydrocarbon chains. According to the Bragg rod analysis (Figure 2D), the thickness of the crystalline part of the film is 21 Å. This value translates into a 16−17 carbon acyl chain length and suggests that one or two carbons of the low part of the chain, connected to the six-membered siloxane ring, do not adopt an all-trans conformation and thus appear disordered in the random tessellation pattern (see below). It is interesting to note that the crystalline thickness established in this study is significantly larger than the one established for the solid support and is attributed to the lateral strain due to cross-links.[21] Our results cast some doubt on this interpretation. Assuming mostly the same trimer structure in both cases, the lower crystalline thickness of the siloxane films on solid supports may be caused by the interactions with the solid support and its roughness. Such interactions can in turn lead to vertical offsets of the neighboring molecules and decreased crystalline thickness of the film.

The long-range crystalline order of the trimers (superstructure) should give rise to low-order reflections that were not observed in the GIXD spectra, thus supporting a random orientation of the trimers within the crystalline film in two opposite orientations (Figure 4D). This structure could be represented as a randomized 2D tessellation pattern (Figure S2). We note that the random tessellation packing of the trimers may have an energetic advantage over the proper crystalline state as it should have higher entropy, whereas their enthalpy should be similar (van der Waals contacts between the trimers). Even though the GIXD analysis suggests that the ordered OTOS structure should be made of cyclic trimers, we cannot rule out the existence of linear polymer chains at the crystal boundaries. Thus, we propose that the overall structure of OTOS films may be a composite of the trimers, constituting most of the ordered film, with some fractions of linear polymer chains at the domain boundaries (see Figure S1).

Our proposed in-plane structure of the OTOS film should have important implications for the former studies of condensed siloxane films both on liquid and on solid supports. For example, *n*-octadecyltrichlorosilane (OTS) undergoes similar chemical transformation and converts into OTOS films after hydrolysis and condensation. It is likely to have the same structure on a solid support after Langmuir−Blodgett deposition or chemisorption, considering that it demonstrates the same lattice spacings as given by AFM, TEM, and GIXD.[24,25] Our model also explains the so-called pseudorotational epitaxy of condensed OTS monolayers on a sapphire surface.[26] Considering that the OTOS film possesses 3-fold symmetry on the level of the siloxane groups, it must have preferential orientation vis-à-vis the sapphire surface of the same 3-fold symmetry.

We now turn to the XR analysis, providing complementary information to the GIXD results. OTOS molecules in the film consist of hydrophobic acyl chains and hydrophilic silicate head groups (Figure 1C), which could be approximated with two electron density boxes. According to XR, the electron density box that corresponds to the hydrocarbon chain region is 21.8(1) Å thick, whereas the box length for the silicate heads is 5.8(1) Å (Table 2, Figures 1C and 2D). The ideal length, *L*, for all-trans hydrocarbon chains of *n* carbons is given by the corrected Tamford formula[27]

$$L(n) = (n - 1)1.27 + 1.5(\text{Å})$$

For OTOS ($n = 18$), the theoretical length is 23 Å, which is about 1 Å longer than the corresponding XR box length. This minor difference could be explained by one gauche defect in the

Table 2. X-ray Reflectivity Models[a]

	length (Å)	density ($e^- Å^{-3}$)	electrons	difference
		OTOS		
heads	5.8 ± 1.0	0.55 ± 0.01	68 ± 8	N/A
tails	21.8 ± 0.8	0.31 ± 0.005	142 ± 12	N/A
total	27.6	N/A	210 ± 15	N/A
		OTOS + $[Zn(NH_3)_4]^{2+}$		
heads	10.7 ± 0.04	0.54 ± 0.05	120 ± 11	52
tails	21.8 ± 0.03	0.32 ± 0.1	148 ± 12	6
total	32.5	N/A	268 ± 16	58

[a]Area per molecule before and after zinc interaction = 21 ± 0.2 $Å^2$.

DOI: 10.1021/jacs.6b05711
J. Am. Chem. Soc. 2016, 138, 12432−12439

acyl chain attached to the six-membered siloxane ring. Electron density of the OTOS headgroup region was found to be 0.544 e^- Å^{-3}, whereas for the acyl chain, the density is 0.31 e^- Å^{-3}. These densities integrated over the defined lengths and multiplied by the area available per average molecule gives the total number of electrons per molecule. Our XR model has 210 e^- per molecule, with 145 e^- in the tail and 65 e^- in the headgroup. The chemical formula for OTOS ($C_{18}H_{37}O_3Si$) predicts 183 e^-, with 145 e^- in the tail group and 38 e^- in the headgroup. The excess 27 e^- within the headgroup in our model could be assigned to three OTOS coordinated water molecules from the subphase. XR modeling results are summarized in Table 2.

2.2. Interaction with Zinc Ions. After hydrolysis and condensation of the OTMS film, the aqueous subphase was injected with ammonium hydroxide to reach pH 10. After 60 min to equilibrate, the OTOS film was examined by XR and GIXD, and it was found to be structurally the same as that at pH 2. In order to study interactions between OTOS and Zn^{2+}, an aqueous solution of zinc nitrate was injected into the aqueous subphase to reach a final concentration of Zn^{2+}:OTOS = 10^4:1 (~1 μM). Under these conditions, zinc ions form tetrahedral complexes of $[Zn(NH_3)_4]^{2+}$.[28]

Introduction of Zn^{2+} to the system had little effect on the lateral organization of the crystalline film, according to GIXD. After the injection of zinc ions, the triplet degenerate Bragg peak slightly shifted to q_{xy} = 1.526 Å^{-1}. No observable higher or lower order reflections were detected, as are typically observed for the rotator phase (Figure 2B).[29] As in the case of pure OTOS, the unit cell contains a single acyl chain with an area of 19.57 Å^2 and dimensions $a = b$ = 4.845 Å and γ = 120°. The lateral coherence length of the diffraction increased with the introduction of ions from 133 to 152 Å (Table 1). The integrated peak intensity did not change significantly. GIXD results are summarized in Table 1.

The electron density profile was assigned a two-box minimal model for XR analysis similar to the pure OTOS film described above. The top box corresponds to the hydrocarbon tails, and the bottom box incorporates both the silica head groups and the zinc ions (Figure 1C, Table 2). The length of the tail region was found to be 21.8 Å, the same as in pure OTOS, whereas the headgroup length increased to 10.66 Å. Acyl chain density was found to be 0.32 e^- Å^{-3}, whereas the average density of the headgroup was 0.537 e^- Å^{-3}. The XR findings are summarized in Table 2.

In this system, zinc ions are the only species with electron density significantly higher than water. Therefore, increased electron density in the headgroup region can be attributed only to the presence of zinc ions at the interface. However, quantitative assessment of zinc content at the interface depends on the state of zinc ions and the degree of hydration.

To obtain an upper bound of zinc concentration at the interface, we assume that all extra electrons come from $[Zn(NH_3)_4]^{2+}$ attached to the OTOS hydroxyl groups, without any electrons from coordinated water molecules. In this case, there would be 1.2 $[Zn(NH_3)_4]^{2+}$ ions for each OTOS molecule. However, binding of solute molecules to a headgroup can be accompanied by up to 50% additional hydration.[30−32] Assuming 50% additional solvation, the ratio would be 0.38:1. Therefore, the ratio of $[Zn(NH_3)_4]^{2+}$ to OTOS can be within a range of 1.2−0.38:1. Previous work on silica supported zinc catalysts estimated a 0.5:1 ratio of bound Zn^{2+} to hydroxyl groups. This appears to be the most likely ratio considering the equal number of positive and negative charges at the interface.

2.3. Distribution of Zinc Ions Determined by XFS. Another estimate of zinc ions bound to the interface was obtained by XFS. The K_α-edge of zinc is 9.659 keV, and the zinc K_α fluorescence line is at 8.637 keV. The fluorescence spectrum consists of three distinct peaks corresponding to the elastic beam energy of 10.0 keV, Compton scattering of 9.675 keV, and zinc signal at 8.637 keV (Figure 5). Using two

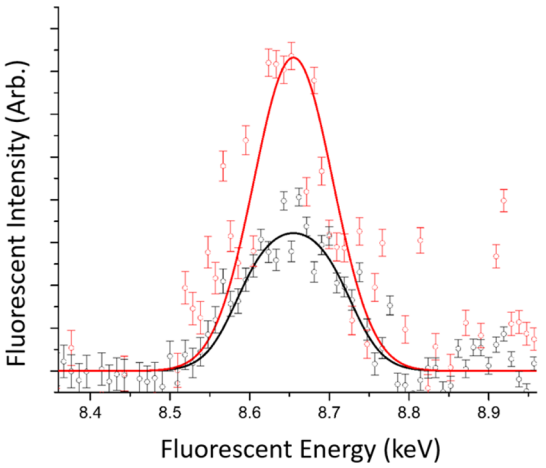

Figure 5. X-ray fluorescence spectroscopy data for 1.5 μM Zn^{2+} subphase without (black circles) and with (red circles) the OTOS monolayer on the liquid surface at q_z = 0.0272 Å^{-1}, along with corresponding Gaussian best fits (solid lines).

samples, with or without the OTOS monolayer on the subphase with equal volume and concentration of zinc ions, we compare the background-subtracted zinc peaks at q_z = 0.0272 Å^{-1} (Figure 5). On the basis of our analysis of the XFS data, we find that the number of zinc ions per OTOS is 0.5:1, consistent with XR analysis. X-ray fluorescence results are presented in Table 3. The modeled OTOS trimer with and without coordinated zinc ions is shown in Figure 1B,C. This molecular model agrees with XR, GIXD, and XFS data.

According to our results, zinc ions demonstrate a high affinity to OTOS trimers. Each OTOS monomer has one free hydroxyl and forms a six-membered siloxane ring within the trimer (Figure 1C). Six-membered rings are a common feature on the surface of solid silica supports.[17] Previous work provided evidence that Zn^{2+} ions were bound exclusively to these rings.[3] The grafting mechanism suggested by our data corroborates that of previous work and is outlined in Figure 6.

This study provides insight into the initial grafting mechanism of $[Zn(NH_3)_4]^{2+}$ onto silica surfaces using a model OTOS monolayer. Our grafting mechanism results agree with those from fully constituted silica-supported Zn/SiO_2 catalysts and provides a better understanding of the grafting mechanisms. Electrostatically bound $[Zn(NH_3)_4]^{2+}$ forms Zn−O bonds with free hydroxyls of six-membered siloxane rings on the surface of silica after heating. This process is consistent with the disappearance of the Raman signal of six-membered siloxane rings at 607 cm^{-1} for a silica-supported single site Zn/SiO_2 catalyst.[3] In this work, zinc ions were found to be coordinated with surface siloxane rings, akin to the mechanism of binding suggested for metal catalysts at silica surfaces. We therefore suggest that this model system allows for near-atomic structural studies of ion coordination *in situ*.

DOI: 10.1021/jacs.6b05711
J. Am. Chem. Soc. 2016, 138, 12432−12439

Table 3. X-ray Fluorescence Spectroscopy Results[a]

	I/I_0 (counts 10^{-6})	concentration (10^{-6} M)	penetration depth (Å)	ions molecule^{-1}
$[Zn(NH_3)_4]^{2+}$, OTOS Film	1.81	1.5	10^5	
$[Zn(NH_3)_4]^{2+}$, bare surface	0.94	1.5	10^5	
ratio	1.94	1	1	0.519 ± 0.2

[a]Area per molecule = 21 Å^2.

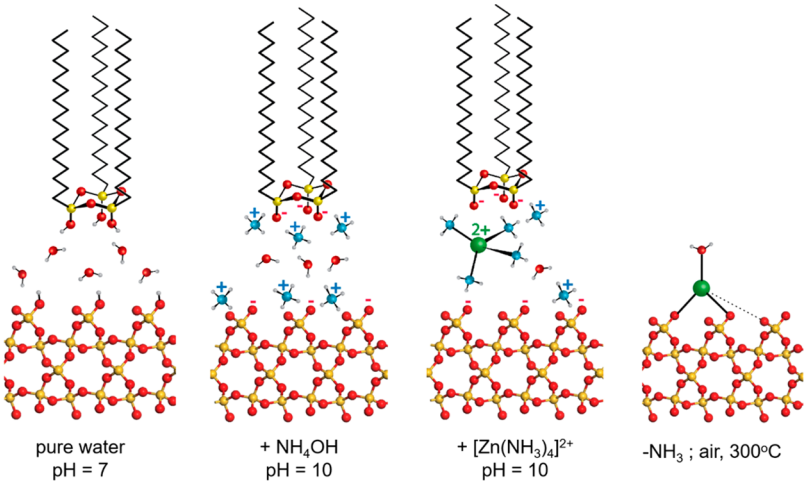

Figure 6. (Top) Suggested model mechanism of grafting of zinc ions under the OTOS film. (Bottom) Corresponding grafting mechanism of zinc ions at the silica interface.

3. CONCLUSIONS

OTMS films at the air−liquid interface undergo hydrolysis and condensation at low pH, forming an ordered film made of cyclic OTOS trimers rather than linear or cross-linked polymers as suggested previously. Each OTOS monomer, which has one free hydroxyl group, forms a six-membered siloxane ring within an OTOS trimer. According to our study, the free hydroxyl groups have high affinity to bind zinc ions. According to XR and XFS, the ratio of zinc ions to free hydroxyls is 0.5 to 1, in agreement with studies of solid-supported silica catalysts. Our approach allows the early adsorption mechanisms of metal ions to silica surfaces to be modeled and monitored. However, more evidence is necessary to establish one-to-one structural correspondence between six-membered silicate rings at the solid silica surface and those that exist in the OTOS film at the air−liquid interface.

4. EXPERIMENTAL SECTION

4.1. Experimental Setup. X-ray measurements on Langmuir monolayer films were carried out in a 25 mL Teflon trough. To reduce the background scattering and protect films from oxidation, the trough was placed into a sealed canister filled with moist helium and equipped with Kapton windows to allow transmission of the X-ray beam. OTMS (Sigma-Aldrich) was dissolved in chloroform to obtain a spreading solution of 0.1 mg mL^{-1}. The aqueous subphase of pH 2.0 was prepared by adding 12 M HCl (Sigma-Aldrich) to Milli-Q water. The OTMS solution was then deposited drop-by-drop onto the liquid surface using a Hamilton syringe until the surface pressure reached 20 mN m^{-1}. Hydrolysis and condensation of OTMS molecules in the film were monitored by changes of the surface pressure, as measured by a Wilhelmy sensor. Within an hour, the surface pressure reached ∼45 mN m^{-1} and then remained constant, indicating the end of the reaction.

To study interactions with Zn^{2+} ions, the liquid subphase was then titrated by adding ammonium hydroxide (NH_4OH) to obtain a pH of 10. Zinc chloride was added to the liquid sub phase with a final concentration of ∼1 μM, allowing for a 1:10000 ratio of surface OTMS to bulk Zn^{2+}.

XR and GIXD measurements were carried out at ChemMatCARS, beamline 15-ID-C, of the Advanced Photon Source (APS) at Argonne National Laboratory (Argonne, IL), using the liquid surface spectrometer described in detail elsewhere.[33] A cryogenically cooled double-crystal Si(111) monochromator was used to select an X-ray wavelength of λ = 1.24 Å, corresponding to a photon energy of E = 10.0 keV, with $\Delta E/E \sim 10^{-4}$. Both XR and GIXD data were collected using a Pilatus 100 K area detector.

4.2. Surface X-ray Studies. According to the standard notation, the incident X-ray beam makes an angle α to the surface plane, and the scattered X-ray beam makes an angle β to the surface and an azimuthal angle ψ to the plane of incidence. In XR measurements, the intensity of the reflected beam ($\beta = \alpha$; $\psi = 0$) is measured as a function of the incident angle α of the wave vector transfer $q_z = (4\pi/\lambda)\sin(\alpha)$ along the surface normal. The background-subtracted intensity was normalized to the incident beam to obtain the reflectivity $R(q_z) = I(q_z)/I_0$, where $I(q_z)$ was measured using a Pilatus 100 K area detector and the monitor counts (I_0) were measured with a gas ionization chamber. XR data processing was done using IDL software. The raw intensity was obtained by integrating the signal in $q_{xy}-q_z$ area for the intervals $-0.25 < q_{xy} < 0.25$ and $-0.05 < q_z < 0.05$. The background was obtained by integrating equal areas for q_{xy} and q_z on either side of the signal corresponding to $-0.75 < q_{xy} < -0.25$ and $0.25 < q_{xy} < 0.75$ with the identical q_z range.[34] For GIXD, the incident angle was set below the surface critical angle at $\alpha = 0.85\alpha_c$ (α_c = 0.0217 Å^{-1}); in-plane diffraction data were collected with the area detector using two vertical slits over a q_{xy} range of 1.0−1.6 Å^{-1}, with $\Delta q_{xy}/q_{xy} = 10^{-2}$ Å^{-1}.

4.2.1. Grazing Incidence X-ray Diffraction (GIXD). GIXD gives information on the lateral order of the film. X-rays at grazing incidence geometry have a low penetration depth of ∼100 Å and are scattered mostly by the ordered Langmuir film, not by the bulk liquid subphase. The d-spacings of the diffracting planes of the ordered film are given by the Bragg peak positions in q_{xy} such that $d_{nm} = 2\pi/q_{xy}(n,m)$. The average size of crystalline domains in the $\{n,m\}$ direction is given by the corresponding crystalline coherence lengths, according to the Sherrer formula (Patterson, 1939)[35]

DOI: 10.1021/jacs.6b05711
J. Am. Chem. Soc. 2016, 138, 12432−12439

$$L_c = (0.9)(2\pi)\left(\frac{1}{\mathrm{fwhm}_i}\right)$$

where fwhm_i is the intrinsic full width at half-maximum of the Lorentzian such that $\mathrm{fwhm}_i = (\mathrm{fwhm}^2 - \mathrm{Res}^2)^{1/2}$, where Res is the resolution of the slits, set at 10^{-2} Å^{-1}. GIXD measurements on the films were performed in a broad range from 0.2 to 3.0 Å^{-1} of q_{xy}.

Bragg Rod Analysis. In 2D crystalline films, the width of intensity distribution along q_z (Bragg rod) is inversely proportional to the thickness the ordered hydrocarbon chains. The hydrocarbon chain could be modeled as cylinder of length L.[36] In such a case, the Bragg rod distribution is given by

$$I(q_z) = I_0 V^2(q_z)(2\pi R^2 L)^2\left(2\frac{J_1(q_{xy}R)}{q_{xy}R}\right)^2 \sin c^2\left(\frac{q_z L}{2}\right) e^{-q_z^2\sigma^2}$$

in which σ is the surface roughness (Å), $J_1(x)$ is the Bessel function of the first kind, R is the radius of the cylinder, q_{xy} is the position of the Bragg rod peak along the parallel axis, $\sin c(x) = \sin(x)/x$, L is the length of the cylinder, and $V(q_z)$ is the characteristic Vineyard function; the wave vector $q_z = 2\pi/\lambda \sin(\beta) + 2\pi/\lambda \sin(\alpha)$ with $\alpha \approx 0$ or $q_z = 2\pi/\lambda \sin \beta$. Considering the hexagonal symmetry of the film, the tilt angle for the chains was fixed to zero, and roughness was to set to a typical value of 1 Å.[36,37] The length of the cylinder L was varied to minimize the difference between $I(q_z)$ function and experimental data.

4.2.2. Specular X-ray Reflectivity (XR). XR determines the electron density distribution across the interface. Typically, solutions to the inverse phase problem are done by dividing the vertical electron density distribution at the interface into a finite number of boxes or slabs, known as the Parratt formalism.[38] Discrete slabs, or boxes, approximate the electron distribution across the interface with exactly solvable densities. Each slab is assigned an error function representing its smoothing or roughness to the adjacent slab. This method allows for the approximate assignment of molecular regions across the interface guided by the known chemical information; for example, the hydrocarbon chains can be modeled as one box with a uniform density of approximately 0.31 e$^-$ Å^{-3}. Slab models offer a simple approximation of the surface electron distribution. Various other model independent methods exist that attempt to invert a density profile from the data, but all of them rely on various restrictions and approximations. A novel approach proposed by Danaskaus et al. that was implemented in the StochFit[39] software involves splitting the electron density profile into a large number of slabs, approximately two per angstrom, and allowing each slab to vary in roughness and density until the modeled reflectivity matches the data by using the greedy search algorithm and χ^2 minimization.

In our study, the method of Danaskus et al.[39] is used in a modified way. The electron density profile is split into many boxes, but the density and roughness of each box are searched over a parameter space by the stochastic tunneling (STUN) search algorithm.[40] The global minimum of the objective function, or reduced χ^2, is found by Monte Carlo sampling. This algorithm is loosely constrained to allow only physically feasible solutions, such that no box may be more than 5% different than the last, ensuring smoothness, and no box may have a density greater than twice the density of water or a lower density than the gas phase (helium gas).

Best-fit models generated by STUN were compared to molecular models created in Accelrys Molecular Studio and Maestro modeling software. We compared the XR modeled lengths and electron densities with the computer generated molecular models and found them to be in good agreement. The STUN electron density profile was fit by a slab model of minimal complexity, i.e., the smallest number of boxes possible with the correct length and integral density that we refer to as a "minimal model". Constraints used in the minimal models were such that the integral electron density of the box model and STUN model were identical. This agreement is ensured by the smoothness condition.[41]

4.5. X-ray Fluorescence Spectroscopy (XFS). XFS was measured using an energy dispersive Vortex-EX silicon multi-cathode detector (SMCD; 51SII NanoTechnology USA, Inc.), positioned normal to the liquid surface, 1 cm above the X-ray illuminated footprint. Resolution of the Vortex detector is approximately 136 eV in the linear detection region, or $\Delta E/E \sim 10^{-2}$. Atoms excited by X-rays of energies above the binding energy edges emit photons spherically with energies given by their K_α transitions. XFS allows for the detection of specific ions at the liquid surface by utilizing a grazing incidence geometry, with a penetration depth of ~50 Å given by the propagation of the evanescent wave.[42] However, quantifying the number of ions per unit area using this geometry is technically challenging. At angles above the critical, XFS probes both the bulk and surface quantities of the liquid. XFS scans were done in a range of incidence angles corresponding to q_z values of 0.0132−0.0282 Å^{-1} for both the system of the OTOS monolayer and a reference sample with no monolayer but identical ion concentration in the bulk subphase. XFS directly measures the concentration of surface ions by comparing ion fluorescence scattering in a sample with an OTOS monolayer and one with a bare interface. In this way, the two signals may be subtracted, leaving only the intensity from the excess surface ions. This is done by recording the intensity from the surface and the bulk, where

$$I_s = CI_0 A\frac{N_{\mathrm{ion}}}{A_{\mathrm{lipid}}}$$

and

$$I_b = CI_0 A\rho_{\mathrm{bulk}} D(\alpha)$$

thus giving

$$\frac{N_{\mathrm{ions}}}{A_{\mathrm{lipid}}} = \left(\frac{I_s}{I_b}\right)D(\alpha)\rho_{\mathrm{bulk}}$$

where I_s is the intensity at the surface, I_b is the intensity of the bulk, C is a proportionality constant, A is the illuminated area, $D(\alpha)$ is the penetration depth of the X-rays, N_{ions} is the number of ions, and ρ_{bulk} is the molar concentration of ions in the bulk. The concentration of ions bound to the OTOS monolayer was evaluated by comparing the two systems, with and without a monolayer, at an angle corresponding to $q_z = 0.0272$ Å^{-1} where the penetration depths, illuminated areas, and ion concentrations in the bulk are equal, thus simplifying the mathematics, as detailed elsewhere.[42]

■ ASSOCIATED CONTENT

Supporting Information

The Supporting Information is available free of charge on the ACS Publications website at DOI: 10.1021/jacs.6b05711.

Scheme of a composite crystal structure of an OTOS monolayer formed mostly by cyclic trimers; examples of periodic and non-periodic tessellation schemes of the OTOS trimer-packing motifs; three structural examples of organosilanes; schematic of the condensation of the OTMS monomers into OTOS trimers at the air−liquid interface; averaged measurements from Cambridge Structural Database for organosilanes (PDF)

Bond distances and angles (XLSX)

■ AUTHOR INFORMATION

Corresponding Authors

*kuzmenko@aps.anl.gov (I.K.)

*ahock@iit.edu (A.H.)

*gidalevitz@iit.edu (D.G.)

Present Address

⊥(B.H.) School of Chemical & Biomolecular Engineering, Georgia Institute of Technology, Atlanta, Georgia 30332, United States.

DOI: 10.1021/jacs.6b05711
J. Am. Chem. Soc. 2016, 138, 12432−12439

Notes

The authors declare no competing financial interest.

■ ACKNOWLEDGMENTS

I.K. thanks Leslie Leiserowitz, Masa Fukuto, David Vaknin, Ben Ocko, and Hans-Georg Steinrück for fruitful discussions. M.W.M is supported by the X-ray Science Division of Argonne National Lab as a Laboratory Graduate Fellow. ChemMatCARS Sector 15 is supported by the National Science Foundation under grant number NSF/CHE-1346572. This research used resources of the Advanced Photon Source, a U.S. Department of Energy (DOE) Office of Science User Facility operated for the DOE Office of Science by Argonne National Laboratory under Contract No. DE-AC02-06CH11357.

■ REFERENCES

(1) Hu, B.; Schweitzer, N. M.; Zhang, G. H.; Kraft, S. J.; Childers, D. J.; Lanci, M. P.; Miller, J. T.; Hock, A. S. *ACS Catal.* **2015**, *5*, 3494.
(2) Hu, B.; Getsoian, A.; Schweitzer, N. M.; Das, U.; Kim, H.; Niklas, J.; Poluektov, O.; Curtiss, L. A.; Stair, P. C.; Miller, J. T.; Hock, A. S. *J. Catal.* **2015**, *322*, 24.
(3) Schweitzer, N. M.; Hu, B.; Das, U.; Kim, H.; Greeley, J.; Curtiss, L. A.; Stair, P. C.; Miller, J. T.; Hock, A. S. *ACS Catal.* **2014**, *4*, 1091.
(4) Pershan, P. S.; Schlossman, M. *Liquid Surfaces and Interfaces: Synchrotron X-ray Methods*; Cambridge University Press, 2012.
(5) Ulman, A. *Adv. Mater.* **1990**, *2*, 573.
(6) Ariga, K.; Okahata, Y. *J. Am. Chem. Soc.* **1989**, *111*, 5618.
(7) Vidon, S.; Leblanc, R. M. *J. Phys. Chem. B* **1998**, *102*, 1279.
(8) Carino, S. R.; Duran, R. S.; Baney, R. H.; Gower, L. A.; He, L.; Sheth, P. K. *J. Am. Chem. Soc.* **2001**, *123*, 2103.
(9) Fontaine, P.; Goldmann, M.; Rondelez, F. *Langmuir* **1999**, *15*, 1348.
(10) Fontaine, P.; Rondelez, F. Kinetics of Polymerisation in Langmuir Monolayers of N-Alkytrimethoxysilane. In *Short and Long Chains at Interfaces*; Daillant, J., Ed.; Editions Frontieres: Gif-sur-Yvette Cedex, France, 1995; p 207.
(11) Blaudez, D.; Bonnier, M.; Desbat, B.; Rondelez, F. *Langmuir* **2002**, *18*, 9158.
(12) Britt, D. W.; Hlady, V. *Langmuir* **1999**, *15*, 1770.
(13) Ulman, A. *Chem. Rev.* **1996**, *96*, 1533.
(14) Carino, S. R.; Duran, R. S. *Macromol. Chem. Phys.* **2005**, *206*, 83.
(15) Carino, S. R.; Underhill, R. S.; Tostmann, H. S.; Skolnik, A. M.; Logan, J. L.; Davidson, M. R.; Culp, J. T.; Duran, R. S. *Langmuir* **2003**, *19*, 10514.
(16) Carino, S. R.; Tostmann, H.; Underhill, R. S.; Logan, J.; Weerasekera, G.; Culp, J.; Davidson, M.; Duran, R. S. *J. Am. Chem. Soc.* **2001**, *123*, 767.
(17) Iler, R. K. *The Chemistry of Silica: Solubility, Polymerization, Colloid and Surface Properties, and Biochemistry*; Wiley: New York, 1979.
(18) Kuzmenko, I.; Kaganer, V. M.; Leiserowitz, L. *Langmuir* **1998**, *14*, 3882.
(19) Kaganer, V. M.; Mohwald, H.; Dutta, P. *Rev. Mod. Phys.* **1999**, *71*, 779.
(20) Sjöblom, J.; Ebeltoft, H.; Bjorseth, A.; Friberg, S. E.; Brancewicz, C. *J. Dispersion Sci. Technol.* **1994**, *15*, 21.
(21) Steinrück, H.-G.; Will, J.; Magerl, A.; Ocko, B. M. *Langmuir* **2015**, *31*, 11774.
(22) Carino, S. R.; Tostmann, H.; Underhill, R. S.; Logan, J.; Weerasekera, G.; Culp, J.; Davidson, M.; Duran, R. S. *J. Am. Chem. Soc.* **2001**, *123*, 767.
(23) Ghaskadvi, R. S.; Ketterson, J. B.; Dutta, P. *Langmuir* **1997**, *13*, 5137.
(24) Kojio, K.; Ge, S.; Takahara, A.; Kajiyama, T. *Langmuir* **1998**, *14*, 971.
(25) Kojio, K.; Takahara, A.; Omote, K.; Kajiyama, T. *Langmuir* **2000**, *16*, 3932.
(26) Steinrück, H.-G.; Magerl, A.; Deutsch, M.; Ocko, B. *Phys. Rev. Lett.* **2014**, *113*, 156101.
(27) Tanford, C. *Proc. Natl. Acad. Sci. U. S. A.* **1974**, *71*, 1811.
(28) Prince, R. *Comprehensive Coordination Chemistry*; Pergamon Press, 1987; Vol. 5, p 925.
(29) Ocko, B. M.; Wu, X. Z.; Sirota, E. B.; Sinha, S. K.; Gang, O.; Deutsch, M. *Phys. Rev. E: Stat. Phys., Plasmas, Fluids, Relat. Interdiscip. Top.* **1997**, *55*, 3164.
(30) Vogel, V.; Mobius, D. *Thin Solid Films* **1988**, *159*, 73.
(31) Ivankin, A.; Kuzmenko, I.; Gidalevitz, D. *Phys. Rev. Lett.* **2012**, *108*, 238103.
(32) Nobre, T. M.; Martynowycz, M. W.; Andreev, K.; Kuzmenko, I.; Nikaido, H.; Gidalevitz, D. *Biophys. J.* **2015**, *109*, 2537.
(33) Schlossman, M. L.; Synal, D.; Guan, Y. M.; Meron, M.; Shea-McCarthy, G.; Huang, Z. Q.; Acero, A.; Williams, S. M.; Rice, S. A.; Viccaro, P. J. *Rev. Sci. Instrum.* **1997**, *68*, 4372.
(34) Meron, M.; Gebhardt, J.; Brewer, H.; Viccaro, J. P.; Lin, B. *Eur. Phys. J.: Spec. Top.* **2009**, *167*, 137.
(35) Patterson, A. *Phys. Rev.* **1939**, *56*, 978.
(36) Als-Nielsen, J.; Kjaer, K. *Phase Transitions in Soft Condensed Matter*; Springer, 1989; p 113.
(37) Smilgies, D. M. *J. Appl. Crystallogr.* **2009**, *42*, 1030.
(38) Parratt, L. G. *Phys. Rev.* **1954**, *95*, 359.
(39) Danauskas, S. M.; Li, D. X.; Meron, M.; Lin, B. H.; Lee, K. Y. C. *J. Appl. Crystallogr.* **2008**, *41*, 1187.
(40) Wenzel, W.; Hamacher, K. *Phys. Rev. Lett.* **1999**, *82*, 3003.
(41) Ramsay, J. O. *Functional Data analysis*; Wiley Online Library, 2006.
(42) Bu, W.; Vaknin, D. *J. Appl. Phys.* **2009**, *105*, 084911.

DOI: 10.1021/jacs.6b05711
J. Am. Chem. Soc. 2016, 138, 12432−12439